

# Anomaly detection for data quality monitoring of the Muon system at CMS

Marco Buonsante<sup>1,2,\*</sup>, Marco Cruciani<sup>3</sup>, Federica Maria Simone<sup>1,4</sup>, and Rosamaria Venditti<sup>1,2</sup> on behalf of CMS collaboration

<sup>1</sup>INFN Bari, Via Giovanni Amendola, 173, 70126 Bari BA

<sup>2</sup>Università degli Studi di Bari Aldo Moro, Piazza Umberto I, 1, 70121 Bari BA

<sup>3</sup>Alma Mater Studiorum - Università di Bologna, Via Zamboni, 33, 40126 Bologna BO

<sup>4</sup>Politecnico di Bari, Via Edoardo Orabona, 4, 70126 Bari BA

**Abstract.** Ensuring the quality of data in large HEP experiments, such as CMS at the LHC is crucial for producing reliable physics outcomes. The CMS protocols for Data Quality Monitoring (DQM) are based on the analysis of a standardized set of histograms offering a condensed snapshot of the detector's condition. Besides the required personpower, the method has a limited time granularity, potentially hiding temporary anomalies. Unsupervised machine learning models, such as auto encoders and convolutional neural networks, have been recently deployed for anomaly detection with per-lumisection granularity. Nevertheless, given the diversity of detector technologies, geometries and physics signals characterizing each subdetector, different tools are developed in parallel and maintained by the sub detector experts. In this contribution, we discuss the development of an automated DQM for the online monitoring of the CMS Muon system, offering a flexible tool for the different muon sub-systems, based on deep learning models trained on occupancy maps. The potential flexibility and extensibility to different detectors, as well as the effort towards the integration of per-lumisection monitoring in the DQM workflow will be discussed.

## 1 Introduction

The Compact Muon Solenoid (CMS) is a multi-purpose detector designed for the study of proton-proton collisions at the Large Hadron Collider (LHC) at CERN.

A sketch of the CMS detector is shown in Fig. 1. CMS is composed of several sub-detectors: silicon trackers (pixel and strips) for particle tracking, electromagnetic and hadron calorimeters for energy reconstruction, all installed inside the CMS superconductive solenoid, as well as the muon chambers outside it. The muon system is composed of four different sub-detectors, based on different gaseous detector technologies: Drift Tubes (DT), Resistive Plate Chambers (RPC), Cathode Strip Chambers (CSC) and Gas Electron Multipliers (GEM). A more detailed description of the CMS apparatus can be found in [1–3].

---

\*e-mail: marco.buonsante@cern.ch

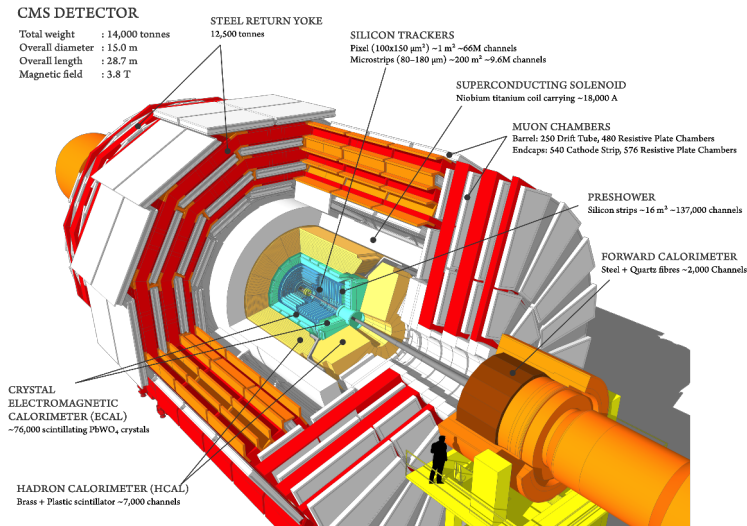


**Figure 1.** Diagram of the CMS detector [4].

### 1.1 Data Quality Monitoring (DQM)

At CMS, data acquisition periods are organized into "Runs", with each Run typically containing between 100 and 1000 Lumisections (LS). LS are the smallest units of data acquisition, defined as the amount of data collected within a 23-second time window.

During CMS data-taking, events are first filtered by the CMS trigger system [5]. Subsequently, a portion of the data stream is utilized in the so-called Online DQM to monitor the detector status and promptly raise alarms. These alarms rely on either automated systems or human visualization of quantities called "Monitoring Elements" (ME), such as histograms, which are filled in real time during the run. After data-taking, the entire dataset is processed to produce similar ME with per-run granularity. These are used in the Offline DQM (see Fig. 2) to provide experts with detailed inputs for investigating potential issues in the detector.

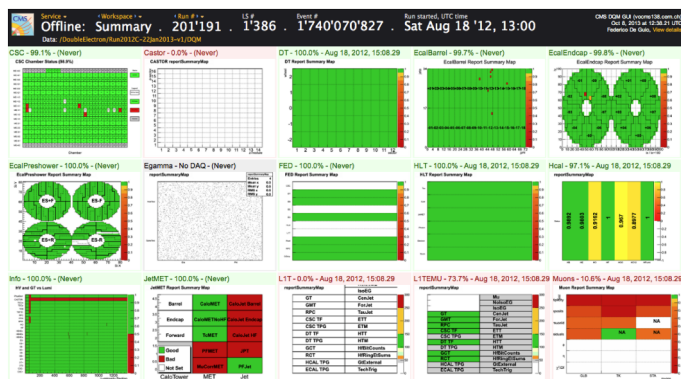


**Figure 2.** An example of the Offline DQM GUI displaying some of the MEs [6].

The Online DQM is a highly time-sensitive operational task, and its main limitation is the

time granularity (Run), which may hide transient issues affecting only a few LSs. To overcome this limitation, the most efficient approach is to adopt a per-LS strategy. However, this change implies an increase in the number of MEs by a factor of  $10^3$ , which makes human inspection unfeasible.

For this reason, there is an ongoing effort within CMS to use Machine Learning (ML) to automate the monitoring of the different subsystems. In this direction, several developments have already been made for ECAL [7], HCAL [8], and the Tracker [9].

## 2 Anomaly detection for the CMS Muon System

Various Anomaly Detection models were tested to identify the most suitable for this use-case. Among them, a ResNet autoencoder was selected due to its simplicity, adaptability to different sub-detectors, and strong capability in both detecting anomalies and localizing them with high precision. Given these advantages, a methodology similar to that adopted by ECAL [7], which has demonstrated good performance for online detector monitoring with per-LS granularity, was chosen as the basis for the development of an automatic anomaly detection tool for the CMS Muon System. This tool leverages occupancy plots from the various sub-detectors of the Muon System (see Section 1) as inputs to a ResNet-based autoencoder. By utilizing the autoencoder’s ability to learn compact and efficient data representations, the approach aims to identify deviations from nominal detector behavior (i.e. anomalies) with high sensitivity and precision.

To demonstrate the applicability of this method to the Muon System, which is characterized by a low particle rate (i.e. low occupancy), a model has been developed specifically for the CSC sub-detector [10], adopting a "few-LS strategy", as will be discussed later.

### 2.1 CSC geometry and expected anomalies

The CSCs are located in the endcaps of the CMS Muon System (see Fig. 3). Each endcap contains four CSC disks, referred to as “stations,” and denoted as  $ME_{\pm X}$  (where  $X = 1, 2, 3, 4$ , and  $\pm$  indicates the positive or negative endcap of CMS). Each station is divided into 2 rings (or 3 rings for station  $ME_{\pm 1}$ ), denoted as  $ME_{\pm X/Y}$ , where  $Y$  indicates the ring number. In addition, each ring is divided into chambers spanning  $20^\circ$  ( $10^\circ$ ) for  $ME_{\pm X/1}$  ( $ME_{\pm X/2}$ ). Each chamber is read out by 5 front-end boards [11].

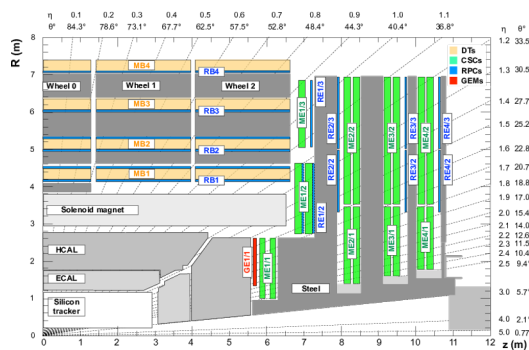


**Figure 3.** View of the CMS detector muon system in the R-z plane [2, 12] (left).

The main expected anomalies in the CSC are excesses or deficits of entries in an entire chamber or in a readout sector.

## 2.2 Data pre-processing

The dataset used to train the autoencoder consists of approximately 150k LSs collected by CMS during proton-proton collisions and certified as GOOD by experts. For each LS, the corresponding CSC occupancy plot (i.e. the distribution of reconstructed hits) for the ME-2 station is considered. These histograms are automatically generated by CMS as part of the data-taking workflow. An example of a CSC occupancy plot is presented in Fig. 4 - left.

As shown in Fig. 4 - left, the Muon System, particularly in the low-eta regions (i.e.,  $ME_{\pm X/2}$ ), is characterized by very low statistics, which makes such type of image unsuitable for model training. To address this, consecutive LSs were summed up to an integrated luminosity of  $7 \text{ pb}^{-1}$ . This threshold is chosen to strike a balance between maintaining fine time granularity and achieving sufficient statistics, thereby implementing the previously mentioned few-LS strategy. An example of the occupancy plots after summation is shown in Fig. 4 - right.

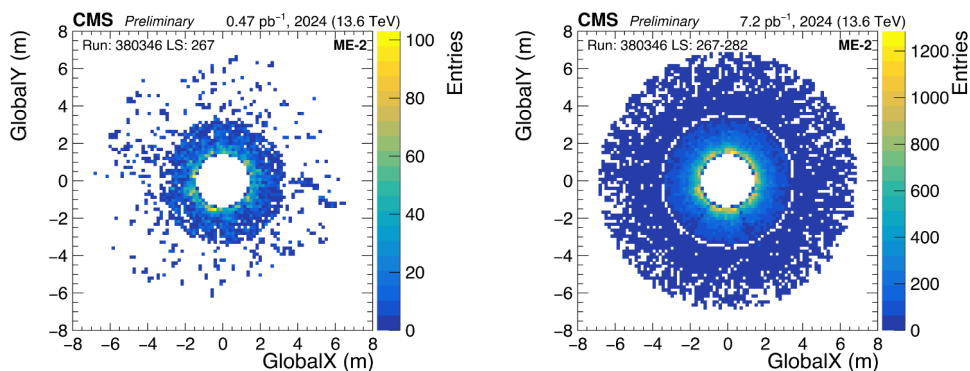


**Figure 4.** Reconstructed hits map in CSC ME-2 for one single LS (left). Reconstructed hits map in CSC ME-2 summing consecutive LSs (right). [10]

Even after this summation, the occupancy of ME-2/2 is very low, and these statistical fluctuations can negatively affect the autoencoder’s ability to generalize effectively. To mitigate this issue, the external region of each image is rebinned into slices along the  $\phi$  coordinate (using the rebinning schema illustrated in Figure 5 - right, following the geometry of the detector’s readout system (see Section 2.1). After this rebinning, the image shown in Fig. 4 - right is transformed, as illustrated in Fig. 5 - left.

## 2.3 Training

After pre-processing, the number of available images (i.e. occupancy plots) is approximately 8k. These images are used to train an unsupervised ResNet algorithm for image reconstruction. The ResNet autoencoder is developed using PyTorch and trained on GPUs at the ReCaS Bari data center. A schematic representation of this neural network is shown in Fig. 6. The loss function used during training is the L1Loss (i.e., the mean of the bin-by-bin differences between the input and the output of the autoencoder). To properly account for the differences between  $ME_{\pm X/1}$  and  $ME_{\pm X/2}$ , two separate algorithms were trained. For this reason, the performance of the two models will be presented separately in the following section.

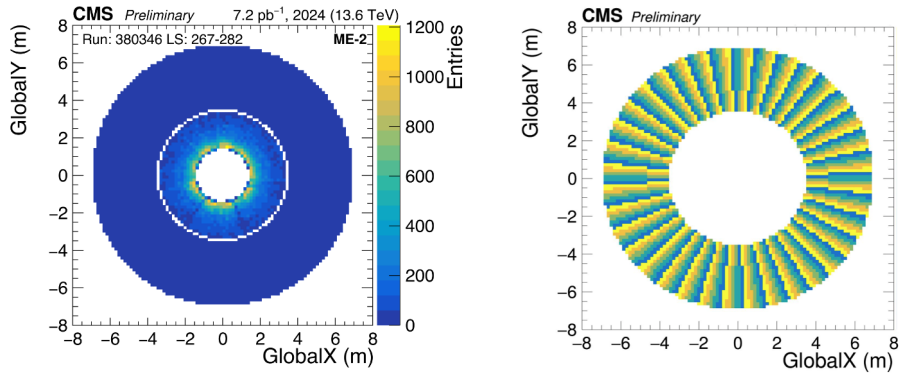


**Figure 5.** Reconstructed hits map in CSC ME-2 after ME-2/2 rebinning (left). Visual representation of the binning scheme applied during rebinning (right) [10]

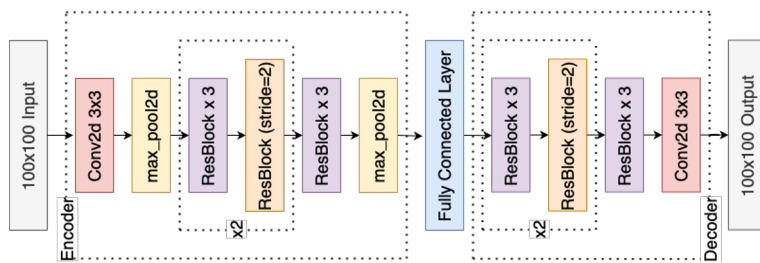


**Figure 6.** Schema of the ResNet architecture.

## 2.4 Validation

To validate the performance of the ME-2/1 training, a set of good and problematic images was isolated from the data through visual inspection. The loss map is then computed as the signed difference between the input and reconstructed images, normalized by the mean of the input images. Subsequently, the distribution of the minimum and maximum loss values is analyzed. The results are presented in Fig. 7.

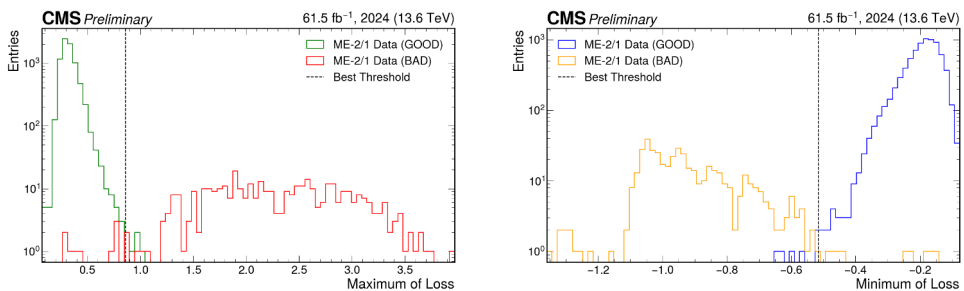


**Figure 7.** Distribution of the maximum (left) and minimum (right) of the loss for good and bad images with thresholds selected maximizing F1 Score for ME $\pm$ X/1. [10]

**Table 1.** Confusion matrix summarizing the performance of the model trained for ME±X/1 in identifying good (Negative) and bad (Positive) occupancy plots

	Positive	Negative
True	99.0%	99.9%
False	0.1%	1.0%

To distinguish between good and bad occupancy plots, thresholds for both the maximum and minimum loss values are chosen to maximize the F1 score<sup>1</sup> [10]. The model’s performance after applying these thresholds is summarized in Table 1.

To validate the performance of the ME±X/2 training, a similar procedure is followed. However, due to the low statistics, it is difficult to visually isolate anomalies. Therefore, artificial anomalies were generated by introducing over/under fluctuations in slices of the detector, based on the geometry of the readout sectors. The same workflow as before is then applied to ME±X/2, leading to the results shown in Fig. 8 and Table 2.

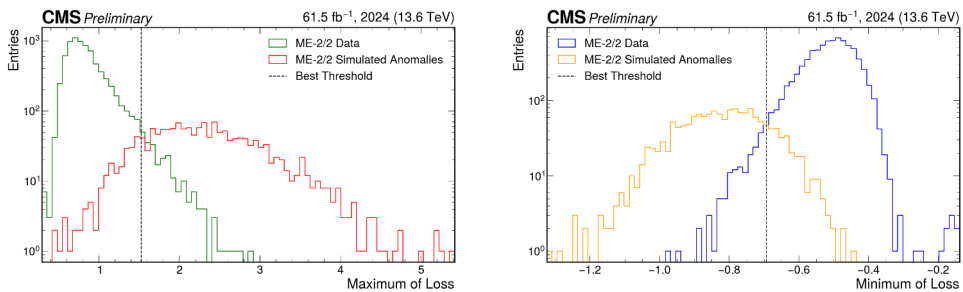


**Figure 8.** Distribution of the maximum (left) and minimum (right) of the loss for good and bad images with thresholds selected maximizing F1 Score for ME±X/2. [10]

**Table 2.** Confusion matrix summarizing the performance of the model trained for ME±X/2 in identifying good (Negative) and bad (Positive) occupancy plots

	Positive	Negative
True	87.6%	95.2%
False	4.8%	12.4%

By applying the thresholds defined in Section 2.4, it is possible to flag anomalous regions in occupancy plots, generating plots that can be used in the final stages by CMS DQM shifters to monitor the detector’s status during data taking. To illustrate how these plots look, a couple of anomalies found in the data are shown in Fig. 9 and Fig. 10.

### 3 Conclusions

To sum up, the applicability of a machine learning-based monitoring to the CMS Muon System has been demonstrated by developing an anomaly detection tool for the online monitoring of the CSC detector, with a time granularity on the order of a few LSs. Anomalies

<sup>1</sup>The "F1 score" is a function of precision ( $p = TP/(TP + FP)$ ) and recall ( $r = TP/(TP + FN)$ ) defined as:  $F1 = 2pr/(p + r)$ , where TP = True Positives, FP = False Positives, and FN = False Negatives.

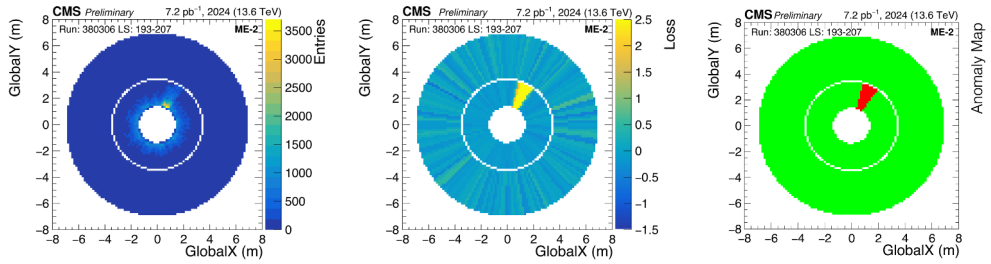


**Figure 9.** Occupancy plot of CSC ME-2 showing high occupancy in one of the ME-2/1 chambers (left). Loss map computed as the difference between the input and the output of the autoencoder, normalized to ensure uniformity along the  $\eta$  coordinate; regions with high (low) loss correspond to areas with an excess (deficit) of entries (center). Anomaly map highlighting the anomalous region (right), identified based on the thresholds defined in Table 1 and Table 2. [10]

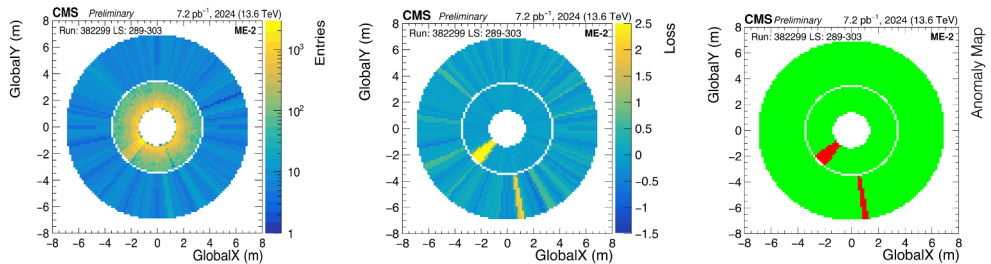


**Figure 10.** Occupancy plot, with log-scale on z-axis, of CSC ME-2 showing high occupancy in one of the ME-2/1 chambers and in some readout sectors of ME-2/2 (left). Loss map computed as the difference between the input and the output of the autoencoder, normalized to ensure uniformity along the  $\eta$  coordinate; regions with high (low) loss correspond to areas with an excess (deficit) of entries (center). Anomaly map highlighting the anomalous region (right), identified based on the thresholds defined in Table 1 and Table 2. [10]

are identified in the 2D occupancy maps of reconstructed hits in the CSC ME $\pm$ X stations. The algorithm was trained on a set of images from certified data, each corresponding to approximately 15 LSs, separately for the ME-2/1 and ME-2/2 rings. After training, a strategy for identifying anomalous images was developed. The algorithm successfully labels 99% of anomalous images for ME-2/1 and more than 85% for ME-2/2 (further optimization ongoing).

This work demonstrates the potential of deep learning models to enhance the efficiency of DQM workflows, paving the way for the application of these tools to the entire CMS Muon System, thanks to their flexibility. As a first step in this direction, the adaptation of this model to the Gas Electron Multiplier (GEM) sub-detector is currently underway, leveraging the same workflow with only minor modifications to the preprocessing. Meanwhile, the feasibility of extending this approach to the remaining Muon System sub-detectors is under evaluation.

## Acknowledgments

This work is partially supported by ICSC — Centro Nazionale di Ricerca in High Performance Computing, Big Data and Quantum Computing, funded by European Union — NextGenerationEU.

## References

- [1] The CMS Collaboration, "The CMS experiment at the CERN LHC". JINST 3 S08004 (2008). <https://dx.doi.org/10.1088/1748-0221/3/08/S08004>
- [2] The CMS Collaboration, "Development of the CMS detector for the CERN LHC Run 3", JINST 19 P05064 (2024). <https://doi.org/10.1088/1748-0221/19/05/P05064>
- [3] J. G. Layter, "The CMS muon project: Technical Design Report". CERN-LHCC-97-032 (1997). <https://cds.cern.ch/record/343814>
- [4] T. Sakuma, "Cutaway diagrams of CMS detector". CMS Collection CMS-OUTREACH-2019-001, 2019. <https://cds.cern.ch/record/2665537>
- [5] The CMS Collaboration, "The CMS trigger system". JINST 12 P01020 (2017). <https://doi.org/10.1088/1748-0221/12/01/P01020>
- [6] Federico De Guio and the CMS Collaboration, "The CMS data quality monitoring software: experience and future prospects", J. Phys. Conf. Ser. 513 032024 (2014). <https://doi.org/10.1088/1742-6596/513/3/032024>
- [7] The CMS ECAL Collaboration, "Autoencoder-Based Anomaly Detection System for Online Data Quality Monitoring of the CMS Electromagnetic Calorimeter", Comput Softw Big Sci 8, 11 (2024). <https://doi.org/10.1007/s41781-024-00118-z>
- [8] The CMS-HCAL Collaboration, "Spatio-Temporal Anomaly Detection with Graph Networks for Data Quality Monitoring of the Hadron Calorimeter", Sensors 2023, 23(24), 9679 (2023). <https://doi.org/10.3390/s23249679>
- [9] The CMS Collaboration, "CMS tracker data quality certification with new machine learning tools", CERN-CMS-DP-2024-070 (2024). <https://cds.cern.ch/record/2905834>
- [10] The CMS Collaboration, "Machine learning tools for the automatized monitoring of the CSC detector", CMS-DP-2024-095 (2024). <https://cds.cern.ch/record/2916189>
- [11] The CMS Collaboration, "Performance of the CMS cathode strip chambers with cosmic rays", Journal of Instrumentation 5, 3 (2010). <https://doi.org/10.1088/1748-0221/5/03/T03018>.
- [12] The CMS collaboration, "Performance of the CMS muon detector and muon reconstruction with proton-proton collisions at  $\sqrt{s} = 13$  TeV", JINST 13 P06015 (2018). <https://doi.org/10.1088/1748-0221/13/06/P06015>